Carbon-13 Nuclear Magnetic Relaxation Study of Solvent Effects on Chain Local Dynamics of Poly(*N*-vinylcarbazole) in Dilute Solution

Aglaia Karali and Photis Dais*

Department of Chemistry, University of Crete, 71409 Iraklion, Crete, Greece

Frank Heatley*

Department of Chemistry, University of Manchester, Manchester M13 9PL, U.K.

Received January 20, 2000

ABSTRACT: Carbon-13 longitudinal relaxation times and NOE values were measured as a function of temperature at three magnetic fields for poly(*N*-vinylcarbazole) (PNVC) in five solvents, covering viscosities differing by a factor of 5. The relaxation data of the backbone carbons were interpreted in terms of chain local motions by using the bimodal time-correlation function of the Dejean−Laupretre−Monnerie (DLM) model. The molecular correlation times obtained from the DLM model follow a linear relationship with solvent viscosity with unit slope, indicating that the hydrodynamic behavior of PNVC can be described by Kramers' theory. Several time-correlation functions describing internal motion failed to reproduce the experimental relaxation data of the protonated aromatic carbons of the carbazole side-group. It was concluded that the internal motion of the carbazole group is highly restricted due to strong steric effects from neighboring rings and the backbone chain. Finally, on the basis of our data some general conclusions were drawn regarding the influence of the backbone rearrangement of PNVC on its photophysical behavior.

I. Introduction

Poly(*N*-vinylcarbazole) (PNVC, **1**) has been the subject

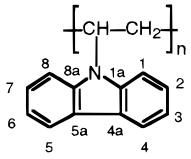

1

of intensive investigation in the last 20 years because of its photoconductive and photophysical properties.[1−7] In particular, photophysical processes of PNVC are unique among vinyl aromatic polymers leading to the formation of two distinct excimer species which clearly depend on the polymer tacticity.[2] However, the influence of the backbone and the side-chain carbazole group motions on the excimer formation has not been considered in previous investigations. The sandwiched parallel disposition of two pendant chromophores and the formation of excimers depend on the chain segmental diffusion and internal rotation about bonds of the side chains. The influence of the chain local motions on excimer formation in this commercially important polymer motivates the present study.

The effect of segmental motion and internal rotation as well as that of tacticity on the intramolecular excimer formation have been examined earlier[8−10] in our laboratories for a series of naphthalene-containing polymers by employing ^{13}C nuclear magnetic relaxation in combination with dynamic modeling. The analysis of ^{13}C NMR relaxation data of these polymer systems showed that the side-chain motion was an important factor for excimer formation. Depending on the side-chain length, excimer formation is confined between nearest naphthyl groups as in poly(1-naphthyl acrylate) and poly(1-naphthylmethyl acrylate) or between next nearest neighbor naphthyl moieties in addition to nearest naphthyl groups as in poly[2-(1-naphthyl)ethyl acrylate]. Solvent effects on the dynamic behavior of these polymer systems have also been studied.[11]

We report here ^{13}C NMR measurements of the local dynamics of PNVC in dilute solution as a function of temperature and magnetic field. Five solvents (tetrahydrofuran, chloroform, dioxane, 1,1,2,2-tetrachloroethane, and pentachloroethane) covering a range of viscosities differing by a factor of 5 are utilized.

II. Experimental Section

Materials. PNVC samples (Aldrich, nominal molecular weight $M_w = 10^6$) were purified by several reprecipitations from chloroform solution using acetone as precipitant. The polymer was studied as solutions of concentration 100 mg cm^{-3} in the deuterated solvents chloroform-*d* ($CDCl_3$), tetrahydrofuran-d_8 (THF), dioxane-d_8, and 1,1,2,2-tetrachloroethane-d_2 (TCE) and the nondeuterated solvent pentachloroethane (PCE). Undegassed samples were used since initial comparisons between degassed and undegassed solutions in $CDCl_3$ showed no measurable difference in the ^{13}C relaxation parameters. The viscosities of all solvents used in this study are known.[12,13]

NMR Measurements. Relaxation experiments were conducted on Varian Associates Inova 300 and 400 spectrometers, and a Bruker Spectrospin AMX500 spectrometer operating respectively at Larmor frequencies of 75.4, 100.5, and 125.7 MHz for ^{13}C. The sample temperature was controlled to within ±1 °C by means of precalibrated thermocouples in the probe inserts.

The longitudinal relaxation times (T_1) were measured by the standard inversion recovery pulse-sequence, and the nuclear Overhauser enhancement (NOE) values were obtained by the inverse gated decoupling technique. The accuracy of the relaxation experiments is estimated to be ±10% and ±15% for the T_1 and NOE values, respectively. The NOE values reported represent averages of at least two measurements at each temperature in each solvent.

It should be noted that the ^{13}C NMR signals of the methine and methylene backbone carbons are split into several components due to tacticity. However, the measured relaxation

10.1021/ma000092c CCC: $19.00
Published on Web 06/30/2000

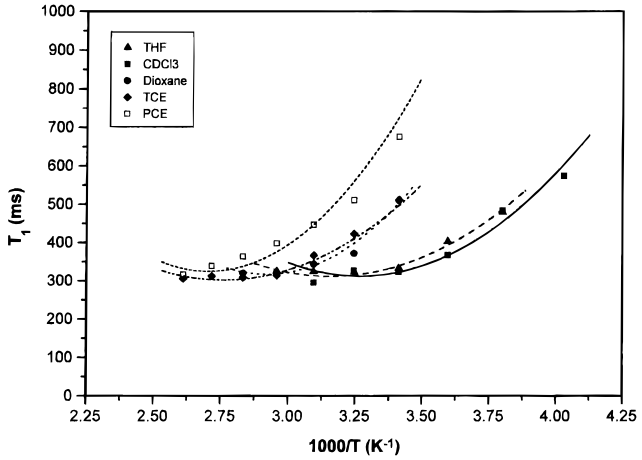

Figure 1. ^{13}C T_1 values for the methine carbon of PNVC in five solvents as a function of temperature at 125.7 MHz. The lines represent the fitting of the T_1 values using the DLM model: (– –) THF; (—) $CDCl_3$; (- – -) dioxane; (—••—) TCE; (•••) PCE.

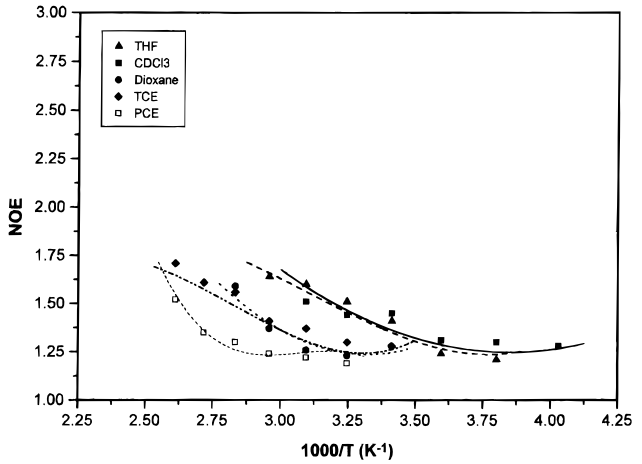

Figure 2. ^{13}C NOE values for the methine carbon of PNVC in five solvents as a function of temperature at 125.7 MHz. The lines represent the fitting of the NOE values using the DLM model. (– –) THF; (—) $CDCl_3$; (- – -) dioxane; (—••—) TCE; (•••) PCE.

parameters of each component within each carbon signal did not differ significantly compared with the estimated experimental error. Therefore, the relaxation parameters for each backbone carbon used in the present analysis represent averages of the relaxation parameters of the various components.

Numerical Calculations. The relaxation data were analyzed by using the MOLDYN program[14] modified by us to include the spectral density function of the motional model used in the present study. Details of the program and the fitting procedure by employing the motional model for the backbone local motions and side-chain motions have been given elsewhere.[14,15]

In the absence of any experimental data on the geometry of PNVC, the C–H bond lengths used in the relaxation analyses were determined from computer conformational calculations on a heptamer of PNVC using the PM3 algorithm in the Gaussian 94 program[16] and the MM+ algorithm in the program HYPERCHEM (Version 5.0, Hypercube Inc.). The calculations gave C–H bond lengths of 1.095 Å for both the methine and methylene backbone groups and 1.08 Å for the aromatic CH groups. These values are consistent with those used previously in similar studies[8,9,11] involving polymers with aromatic side groups.

III. Results and Discussion

Analysis of the NMR Relaxation Data of the Backbone Carbons. The behavior of the experimental relaxation parameters with respect to temperature, magnetic field and solvent is shown in Figures 1–4. Figures 1 and 2 show the NT_1 and NOE values of the methine backbone carbons in five solvents, which are plotted as a function of temperature at 125.7 MHz. (N is the number of directly attached protons.) In Figures 3 and 4 the NT_1 and NOE values of the methine carbon in TCE solvent are plotted as a function of temperature at three magnetic fields. Similar plots are obtained for the methine carbon in the other four solvents, as well as for the backbone methylene carbon. The authors can provide upon request tabulated data at all frequencies and temperatures.

The experimental relaxation data show a number of characteristics commonly observed in the ^{13}C relaxation data of most polymeric materials:[17,18]

(1) As the temperature decreases, the NT_1 values decrease monotonically, in all fields, reaching a minimum which is followed by an increase in NT_1 with further decrease in temperature.

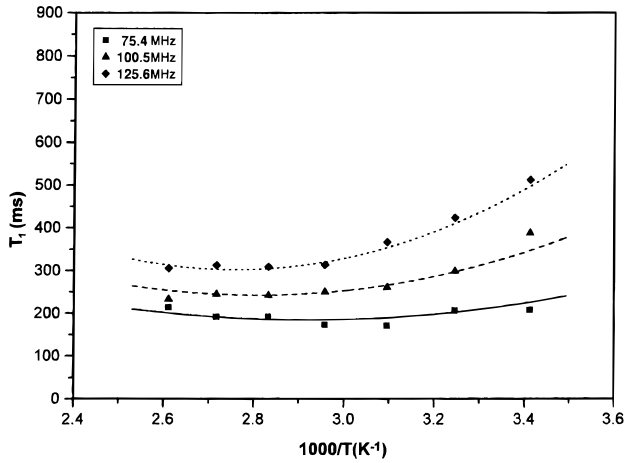

Figure 3. ^{13}C T_1 values for the methine carbon of PNVC in TCE solution as a function of temperature and magnetic field. The lines represent the fitting of the T_1 values using the DLM model. (—) 75.4 MHz; (– –) 100.5 MHz; (---) 125.7 MHz.

(2) The temperature of the minimum in the NT_1 vs temperature curve depends on the solvent.

(3) In a given solvent, the minimum is shifted to higher temperatures (shorter correlation times) as the magnetic field increases.

(4) At a given temperature and solvent, NT_1 values increase with increasing magnetic field, the difference in NT_1 values between the two magnetic fields becoming more pronounced as the temperature decreases (slow motion regime).

(5) The NOE values decrease with increasing magnetic field, although they tend to converge as temperature decreases reaching the slow motion regime.

(6) Both NT_1 and NOE transitions are much broader than for small molecules.

(7) At high temperatures, where motion becomes faster, NOE values are less than the theoretical maximum.

An interesting feature of the data is that in each solvent and at a given magnetic field, the ratio of NT_1 values of the CH and CH_2 groups, $NT_1(CH)/NT_1(CH_2)$, is fairly constant throughout the temperature range studied. This value is constantly lower than unity, which is expected from the number of directly bonded protons,

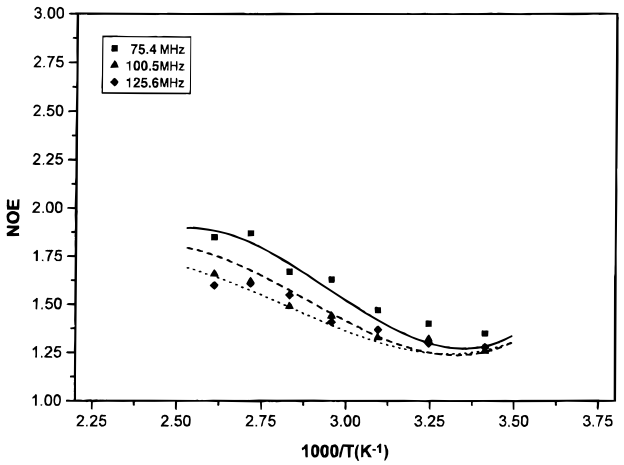

Figure 4. ^{13}C NOE values for the methine carbon of PNVC in TCE solvent as a function of temperature and magnetic field. The lines represent the fitting of the NOE values at different magnetic fields using the DLM model. (—) 75.4 MHz; (— —) 100.5 MHz; (---) 125.7 MHz.

and suggests different local motions for the C−H internuclear vectors associated with the CH and CH_2 groups.

Detailed information on the nature of the intramolecular processes occurring in PNVC is obtained from a quantitative interpretation of the NMR relaxation parameters through dynamic modeling. In modeling the dynamics of PNVC polymer two types of motion are considered: (1) the overall rotatory diffusion of the polymer chain as a whole and (2) chain local motions. Each of these motions is considered as an independent source of motional modulation of the $^{13}C-^{1}H$ dipole−dipole interactions for the protonated carbons of PNVC.

In polymers, the dominant relaxation process for protonated carbons is through $^{13}C-^{1}H$ dipolar interactions.[17,18] Also, for these systems, only interactions with directly bonded protons need be considered. Under conditions of continuous proton decoupling, the ^{13}C relaxation parameters T_1 and NOE can be written in terms of the spectral density function, $J(\omega_i)$, as follows:[17,18]

$$\frac{1}{T_1} = \frac{\Omega}{10}[J(\omega_H - \omega_C) + 3J(\omega_C) + 6J(\omega_H + \omega_C)] \quad (1)$$

$$\mathrm{NOE} = 1 + \left(\frac{\gamma_H}{\gamma_C}\right)\left(\frac{\Omega T_1}{10}\right)[6J(\omega_H + \omega_C) - J(\omega_H - \omega_C)] \quad (2)$$

Here

$$\Omega = N\left(\frac{\mu_0 \gamma_H \gamma_C h}{8\pi^2 r_{CH}^3}\right)^2$$

and γ_H and γ_C are the magnetogyric ratios of proton and carbon nuclei respectively, ω_H and ω_C are their Larmor frequencies, m_0 is the vacuum magnetic permeability, h is Planck's constant, N is the number of directly bonded protons, and r_{CH} is the C−H internuclear distance. $J(\omega_i)$ is related to the normalized time−correlation function (TCF), $G(t)$, which is one projection of the information about mechanisms and rates of the various motional processes.

$$J(\omega) = \frac{1}{2}\int_{-\infty}^{+\infty} G(t)\, e^{i\omega t}\, dt \quad (3)$$

The assumption of independent motions allows the total TCF to be expressed as a product of the TCFs associated with each motional process. As we shall see below the various degrees of freedom of the PNVC chain occur in well-separated time scales justifying the factorization of the corresponding TCFs.

The chemical shift anisotropy mechanism (CSA) is expected to contribute to the relaxation of the aromatic carbons of the carbazole moiety at high magnetic fields. Equations 1 and 2 can be modified to include this contribution:

$$\frac{1}{T_1^{obs}} = \frac{1}{T_1^{DD}} + \frac{1}{T_1^{CSA}} \quad (4)$$

Here T_1^{DD} is the dipole−dipole contribution as in eq 1, and T_1^{CSA} represents contributions from the chemical shift anisotropy mechanism. If the chemical shift tensor is axially symmetric, T_1^{CSA} is given by[9,17,19]

$$\frac{1}{T_1^{CSA}} = \left(\frac{2}{15}\right)\omega_C^2 \Delta\sigma^2 J(\omega_C) \quad (5)$$

with

$$\Delta\sigma = \sigma_{33} - \frac{1}{2}(\sigma_{11} + \sigma_{22}) \quad (6)$$

where σ_{ii} are the principal components of the diagonalized chemical shift anisotropy tensor. The NOE is given by eq 7 upon combining eqs 1, 2, 4, and 5:

$$\mathrm{NOE} = 1 + \left(\frac{\gamma_H}{\gamma_C}\right) \times \left\{\frac{\left(\frac{\Omega}{10}\right)[6J(\omega_H + \omega_C) - J(\omega_H - \omega_C)]}{\left(\frac{\Omega}{10}\right)[J(\omega_H - \omega_C) + 3J(\omega_C) + 6J(\omega_H + \omega_C)] + \left(\frac{2}{15}\right)\omega_C^2 \Delta\sigma^2 J_1(\omega_C)}\right\} \quad (7)$$

The use of eqs 4−7 is an approximation, since the chemical shift tensor of the protonated carbons of the carbazole group may not be axially symmetric. Experimental chemical shielding tensors for carbazole rings did not appear to be available in the literature, so the chemical shielding anisotropy was obtained from GIAO NMR calculations for carbazole and its *N*-methyl and *N*-ethyl derivatives.[20] The high frequency principal components of the tensors were found to be directed approximately along the C−H bonds,[20] indicating that one of the vectors whose motion leads to CSA relaxation is nearly parallel to the C−H bond. In the present calculations, higher order effects were ignored and the relaxation data were fitted to eqs 4−7 with values for $\Delta\sigma$ of 160 ppm for C-1 and 180 ppm for C-2 from the GIAO calculations. These values are similar to the value of 167 ppm used previously for relaxation of the aromatic carbons in naphthyl acrylates;[9,11] this value was derived from experimental data for naphthalenes.

For sufficiently high molecular weight random coil polymers (above a critical value of 1000−10000 depending on chemical structure), the overall motion is much slower than the chain local motions and thus makes a small contribution to the relaxation of the backbone and

side chain carbons.[17,18] The molecular weight of the present PNVC sample lies well above this limit. Thus, the results reported here should represent the PNVC behavior in the high molecular weight limit. The reported relaxation parameters are therefore dominated by local polymer dynamics.

Earlier investigations[17,18] on chain local motions for polymers in solution have concluded that the bimodal dynamic model developed by Dejean de la Batie, Lauprêtre, and Monnerie[21] (DLM) is successful in describing the relaxation data of the backbone carbons. This model will be employed here to describe the chain local dynamics of PNVC. It describes the backbone reorientation in terms of two independent kinds of motion: (1) a diffusional process along the chain, which occurs via conformational transitions described by two correlation times τ_0 and τ_1, for isolated, single-bond conformational transitions and for cooperative transitions, respectively, and (2) bond librations, i.e., wobbling in a cone motion of the backbone internuclear C−H vectors. The librational motion is associated with a correlation time, τ_2, whereas the extent of the libration about the rest position of the C−H bond (the axis of the cone) is determined by the cone-half-angle θ. Combining these two models, the composite DLM spectral density is given by[21]

$$J(\omega) = \frac{1 - A}{(\alpha + i\beta)^{1/2}} + \frac{A\tau^2}{1 + \omega^2\tau_2^2} \qquad (8)$$

with

$$\alpha = \frac{1}{\tau_0^2} + \frac{2}{\tau_0\tau_1} - \omega^2 \qquad \beta = -2\omega\left(\frac{1}{\tau_0} + \frac{1}{\tau_1}\right)$$

$$1 - A = \left[\frac{\cos\theta - \cos^3\theta}{2(1 - \cos\theta)}\right]^2$$

The time constant τ_2 in the second term of eq 8 is short compared to the inverse of the Larmor frequency. For very fast librations compared to segmental motions ($\tau_2 \ll \tau_1 < \tau_0$), the second term in eq 8 contributes very little to the spectral density function and can be neglected from the calculations. The range spanned by $(\tau_0^{-1} + 2\tau_1^{-1})^{-1}$ and τ_0 determines the width of the distribution.

The simulation parameters of the DLM model that reproduce the experimental data of PNVC in the five solvents and at three magnetic fields are listed in Table 1. The best fit of NT_1, and NOE data is plotted in Figures 1−4 for the methine backbone carbon of PNVC. The agreement between experimental and theoretical values is very good throughout the entire temperature range studied and reflects the ability of the DLM dynamic model adopted to describe the backbone motions of PNVC in the five solvents. Similar good fits are obtained for the methylene backbone carbon.

The ratios τ_0/τ_1 and τ_1/τ_2 are fairly constant in each solvent. It should be noted that the same results of the fits are obtained by assuming τ_2 to be constant with a value of 1 ps. Experimental results[11,22,23] and theoretical calculations[24] have shown that the fast librational motion is temperature and viscosity independent.

In all solvents, the best fit half-angles of the librational motion of the C−H vectors at the methine carbon, θ_{CH}, are smaller than the corresponding half-angles of the methylene carbons, θ_{CH_2} (see Table 1). This observation explains the fact that the ratio $NT_1(CH)/NT_1(CH_2)$ is less than unity, and supports the conclusion that θ is related to the steric hindrance at the considered site: the larger the steric hindrance, the smaller is θ. The methine carbon has a directly attached carbazole unit, which, because of its size, physically restricts the amplitude of the local libration. This observation is in agreement with other studies[9,11,25,26] reporting correlations between libration amplitude and side-group mass.

Table 1. Simulation Parameters for PNVC Using the DLM Model

	τ_1 (ns)				
T (°C)	$CDCl_3$	THF	dioxane	TCE	PCE
−25	5.48				
−10	3.53	3.95			
5	1.88	2.48			
20	1.46	1.42	4.27	4.31	6.99
35	1.06	1.08	2.19	3.18	4.60
50	0.78	0.82	1.91	2.01	3.24
65		0.66	1.31	1.34	2.35
80			0.78	1.00	1.66
95				0.78	1.27
110				0.69	0.86
τ_0/τ_1	20	30	20	25	30
τ_1/τ_2	280	300	300	200	300
$\theta_{CH_2\,(deg)}$	26	25	27	26	27.5
$\theta_{CH\,(deg)}$	22.5	22	22	21	22.5
E_a (kJ mol^{-1})	17.5	17.5	23	20.5	21.5
R	0.99	0.99	0.98	0.99	0.99
E_h (kJ mol^{-1})	7.5	8	12.5	12.5	13
E^* (kJ mol^{-1})	10	9.5	10.5	8	8.5

It is of interest to note that both θ_{CH} and θ_{CH_2} values are independent of solvent viscosity. These values are similar in the five solvents ($\theta_{CH} = 22°$ and $\theta_{CH_2} = 26.5°$ on the average). This observation is consistent with the fact that librational motion is a much faster motion than backbone conformational transitions, and hence it is only very weakly dependent on solvent viscosity as mentioned previously. In the absence of specific solvent−polymer interactions, the solvent molecules move only slightly on the librational time scale, imposing no appreciable friction to the librational motion of the backbone C−H vectors.

Kramers' Theory and Viscosity Effect on PNVC Local Dynamics. The τ_1 values derived from fitting the experimental relaxation data of PNVC with the DLM model in the five solvents are compiled in Table 1. Plots of the logarithm of these values as a function of $1/T$ show linear correlations in the temperature range studied, yielding apparent activation energies, E_a, of 17.5, 17.5, 23, 20.5, and 21.5 kJ mol^{-1} for chloroform, THF, dioxane, TCE, and PCE solvents, respectively. These values are summarized in Table 1 along with the correlation coefficients of the Arrhenius plots. Subtracting the activation energy of the viscous flow, E_η, from the apparent activation energy (eq 9), the potential barrier height, E^*, to the conformational transition of the PNVC chain in the various solvents can be calculated[11,27] from the equation

$$E^* = E_a - E_\eta \qquad (9)$$

The calculated values of E^* are 10, 9.5, 10.5, 8, and 8.5 kJ mol^{-1} for chloroform, THF, dioxane, TCE, and PCE solvents, respectively. The value of E_η for each solvent used in eq 9 was obtained from plots of log η vs $1/T$ and are summarized in Table 1.

Equation 9 assumes that Kramers' theory is valid. Kramers' theory[28] describes the rate at which a particle

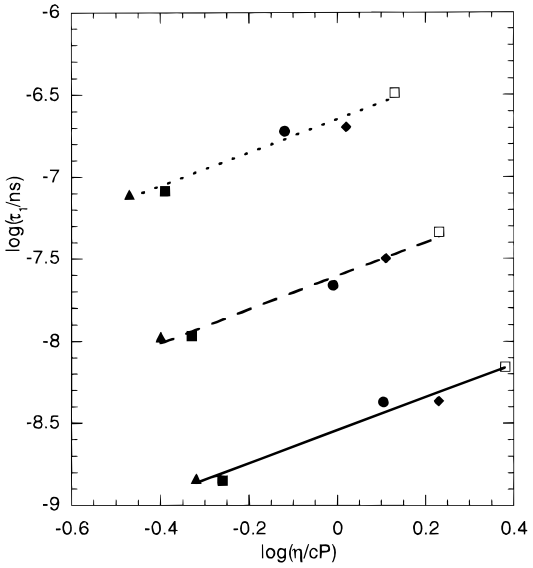

Figure 5. Dependence of log τ_1 on log η for PNVC at three temperatures (eq 10). (—) 20 °C; (— —) 35 °C; (---) 50 °C. The symbols represent different solvents: ▲, THF; ■, $CDCl_3$; ●, dioxane; ◆, TCE; □, PCE. For clarity, the values of log τ_1 at 35 and 50 °C have been raised by one and two units, respectively. The slopes of the three lines are very close to unity (1.01 ± 0.1).

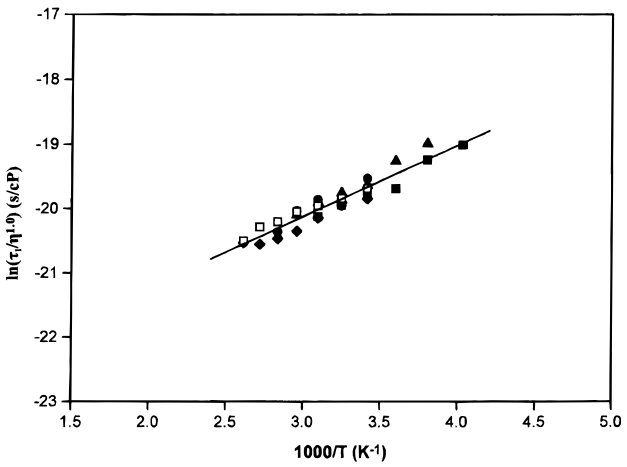

Figure 6. (a) Temperature dependence of τ_1 for PNVC scaled with solvent viscosity η according to eq 10. The symbols represent different solvents as in Figure 5. A large number of data lie on a single universal curve indicating the validity of Kramers' theory in describing the hydrodynamic behavior of PNVC in dilute solutions.

passes over an energy barrier under the influence of Gaussian random forces. It has been often applied to polymer local dynamics in dilute solutions. In this context, and in the high friction limit, Kramers' theory predicts that the viscosity dependence of the correlation time is linear, according to the equation

$$\tau_1 = C\eta \exp(E^*/RT) \qquad (10)$$

where C is a constant, and η is the solvent viscosity. Any deviation from unit slope in the plot of log τ_1 vs log η which may be observed especially at high viscosities, indicates that Kramers' expressions (9) and (10) are insufficient to describe the experimental relaxation rates. Equation 10 has been tested in Figures 5 and 6. In Figure 5, log τ_1 is plotted as a function of log η at three constant temperatures for which correlation times are available for all solvents. (Note that for clarity, the values of log τ_1 at 35 and 50 °C have been raised by one and two units, respectively.) The data for five solvents at each temperature fall on a straight line. The slopes of these lines in Figure 5 are very close to unity as predicted by eq 10, namely 0.98 ± 0.09 at 20 °C, 0.98 ± 0.06 at 35 °C, and 0.98 ± 0.09 at 50 °C. It appears that eq 10 is capable of describing the viscosity dependence of τ_1 at constant temperature. It should be noted that this procedure assumes that the value of E^* is the same in all solvents.

A more rigorous test of the Kramers' equation is shown in Figure 6, where the correlation times scaled by the solvent viscosity for each solvent are plotted as a function of temperature. Although not perfect, Kramers' theory provides a reasonable fit to the experimental data. The average E^* calculated by using eq 9 is 9.1 ± 0.3 kJ mol^{-1}. Note that this value is very close the E^* values obtained from eq 9.

The success of Kramers' theory in explaining the hydrodynamic behavior of PNVC signifies the validity of its major hypothesis that solvent−polymer collisions are uncorrelated in space and time at the high friction limit. This means that conformational transitions of the PNVC chain are slow enough to allow the solvent molecules at each point along the reaction coordinate to equilibrate to the new positions of the chain atoms. In these circumstances, the friction impeding the conformational transition of the polymer chain is proportional to the zero frequency solvent viscosity and the high-friction Kramers' theory is applicable. Zhu and Ediger[30] have shown that Kramers' behavior is expected for large side-groups as in the present case. However, there are several cases[11,21,22,29,30] where motion of the solvent molecules near the top of the barrier takes place on a very short time scale (picoseconds or subpicoseconds). In this case, motions may be significantly correlated, and the time scales for polymer and solvent motions are not cleanly separated.

Frequency−Temperature Superposition. Additional proof of the validity of Kramers' theory in describing segmental motion of PNVC is offered by the principle of frequency−temperature superposition.[31] This principle is accurate provided that all molecular processes that influence the relaxation parameters T_1 and NOE at different Larmor frequencies have the same temperature dependence. Following the procedure of Guillermo et al.,[31] we plot log[$NT_1(T)/\omega_C$] vs log[$\omega_C\tau_1(T)$], where $T_1(T)$ and $\tau_1(T)$ are the values of T_1 and τ_1 at temperature T (Table 1). Similarly, we plot NOE vs log[$\omega_C\tau_1(T)$]; the results for all solvents and magnetic fields are shown in Figure 7. A large number of NT_1 and NOE data for the methine carbon are successfully superimposed in five solvents and various magnetic fields over the entire temperature range studied. These results indicate that indeed Kramers' theory is valid for describing the hydrodynamic behavior of PNVC in dilute solutions. Also, these results indicate that for PNVC over this range of temperatures and frequencies, the shape of the DLM time correlation function is approximately constant.

Two points should be stressed here relative to the frequency−temperature superposition procedure. First, the correlation time τ_2 is considered temperature-independent, and hence does not influence the shape of the DLM function. Second, the frequency−temperature superposition is not dependent on any particular time-

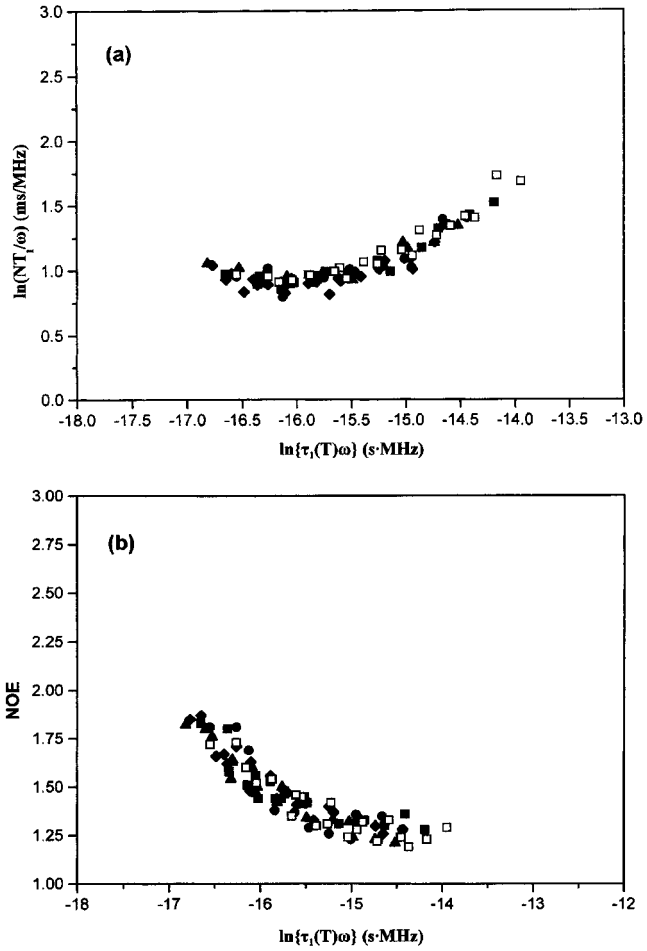

Figure 7. Frequency−temperature superposition plots of (a) T_1, and (b) NOE values at different magnetic fields.

correlation function. It works well with any particular model provided that the correlation times of the model show the same temperature dependence.

Side-Chain Motion. Internal rotation of side groups attached to the polymer backbone, such as phenyl or naphthyl groups, affects the relaxation of the aromatic carbons as a result of the different orientations of their C−H internuclear vectors relative to the internal axis of rotation.[8,17] Assuming that the axis of internal rotation coincides with the bond connecting the side-group group with the main chain of the polymer, a C−H vector parallel to the axis of internal rotation will not be affected by the internal motion, whereas internuclear vectors making an angle β ($\beta \sim 60°$ for phenyl or naphthyl groups) with this axis are expected to be influenced by internal rotation.[8,17] In this respect, the aromatic carbons of carbazole moiety are classified into three groups depending on the angle β formed by the corresponding C−H vectors with the internal axis of rotation, the latter assumed to be coincident with the bond N−C connecting the carbazole group with the main chain of the PNVC polymer. The C−H vectors in each group form similar angles β. The first group contains carbons C-1, C-4, C-5, and C-8 with $\beta \sim 16°$, the second is formed by carbons C-2 and C-7 with $\beta \sim 75°$, and the members of the third group are carbons C-3 and C-6 with $\beta \sim 46.5°$. Carbons in each group must show similar relaxation parameters within experimental error, whereas different relaxation parameters are expected for carbons belonging to different groups. Among

Table 2. Experimental T_1 (ms) and NOE of the Methine Backbone Carbon and Aromatic Carbons of PNVC in $CDCl_3$ Solutions

	CH		C-1, C-5, C-8		C-2, C-7	
T (°C)	T_1	NOE	T_1	NOE	T_1	NOE
			75.4 MHz			
−25	283	1.23	282	1.17	269	1.27
−10	204	1.31	203	1.20	212	1.30
5	196	1.44	199	1.37	207	1.42
20	187	1.44	191	1.45	191	1.46
35	196	1.58	189	1.61	192	1.67
50	200	1.83	196	1.68	200	1.82
			100.5 MHz			
−25	419	1.33	367	1.26	352	1.22
−10	325	1.36	301	1.29	303	1.24
5	267	1.42	264	1.30	241	1.28
20	271	1.48	252	1.37	236	1.34
35	248	1.56	230	1.43	215	1.40
50	246	1.80	224	1.54	210	1.50
			125.7 MHz			
−25	574	1.28	482	1.23	432	1.18
−10	484	1.30	370	1.27	345	1.20
5	367	1.31	312	1.29	293	1.21
20	323	1.44	280	1.37	253	1.28
35	327	1.45	270	1.37	249	1.30
50	295	1.51	258	1.44	239	1.36

the various carbon signals in the ^{13}C NMR spectrum of PNVC, only carbons C-1, C-5, and C-8 from the first group are resolved, whereas C-2 and C-7 carbon signals from the second group overlap.[32] The signal of carbon C-4 overlaps with those of carbons C-3 and C-6. Therefore, the relaxation parameters of the latter carbons cannot be measured with accuracy, and are not considered in the present discussion. The experimental relaxation parameters T_1 and NOE of carbons in the first group (C-1, C-5, and C-8) are the same within experimental error. Carbons C-2 and C-7 overlap, but are expected to show similar relaxation data.

Table 2 summarizes the experimental relaxation data of the methine backbone carbon of PNVC with the average relaxation parameters of carbons in the first and second group measured in chloroform solvent. Inspection of Table 2 reveals that the average relaxation parameters of the aromatic carbons are almost the same as those of the methine carbon at 75.4 MHz, but they become smaller as the magnetic field increases. This observation reflects the increasing contribution of the chemical shift anisotropy mechanism to the relaxation of the aromatic carbons as the magnetic field increases (see eqs 4−7). Comparing the average relaxation parameters of the aromatic carbons of the two groups we observe that these values are not very different within experimental error at all temperatures and magnetic fields. The smaller differences are observed at 75.4 MHz (from 1.8% to 4.5%), and the highest at 125.7 MHz (from 6% to 10%). This difference is intermediate at 100.6 MHz (from 1% to 7%). Similar trends in the relaxation data are observed in the other four solvents.

As inspection of the relaxation data among the aromatic carbons in Table 2 reveal differences within the experimental error, and as these values are comparable or smaller than the relaxation parameters of the backbone methine carbon, we conclude that the carbazole internal rotation is highly restricted. Indeed, any attempt to quantify the relaxation data of the aromatic carbons using several composite time-correlation functions describing restricted internal rotation superimposed on chain segmental motions,[17] the latter

being described by the DLM model, and involving a contribution from chemical shift anisotropy through eqs 4−7, was unsuccessful.

General Remarks on Excimer Formation in PNVC. The photophysical properties of PNVC polymer are unique among vinyl aromatic polymers. Time-resolved fluorescence studies[1−7] of PNVC in solution reveal the formation of two distinct intramolecular excimers, the first a true sandwich excimer near 420 nm, and a second excimer of less clear structure near 370 nm. The first excimer is formed when two carbazole groups have achieved a fully overlapping, sandwich-like arrangement, whereas for the formation of the second excimer a partial overlap of two carbazole groups has been invoked. Emission from the true excimer is relatively more intense in a more isotactic polymer, while the formation of the second excimer has been associated with syndiotactic stereochemical sequences. Thus, tacticity is an important factor in the relative abundance of these two types of excimers.[2,33]

Both conformational and dynamic factors will play a role in determining the photophysical behavior of PNVC. From a ^{1}H NMR study of *meso* and *racemic* 2,4-di-*N*-carbazoylpentanes,[34] it was concluded that for the *meso* isomer the predominant conformations by far were the (equivalent) *tg* and *gt* conformations, whereas for the *racemic* isomer, the lowest energy conformation was the *tt* conformation, the *gg* conformation lying some 2.3 kJ mol^{-1} higher. Conformational energy calculations[35] indicate that these *meso* conformations are also the favored conformations for isotactic dyads in the polymer, though they possibly suggest a higher population of the *tt* conformation, while for syndiotactic dyads, the *tt* conformation is even more preferred. (The conformational notation used is that of ref 35.) From time-resolved absorption spectra in the picosecond and nanosecond time range on the 2, 4-dicarbazoylpentane models, it has been proposed[4,6,33] that the second excimer arises from partial overlap of the carbazole rings created from a slight rotation of ca. 20° of the backbone bonds in the *tt* conformation[32] of a syndiotactic dyad: see Figure 8a. Thus, the formation of the second excimer is very fast (less than 2 ns), and is characterized by a low activation energy. The true excimer, being formed by full overlap of neighboring carbazoyl groups, requires eclipse of the chromophores on the same side of the backbone. Such an arrangement exists in the *tt* conformation of an isotactic dyad and in the $t\bar{g}$ and $\bar{g}t$ conformations of a syndiotactic dyad, but formation of these conformations requires a 120° rotation about backbone C−C bonds from the lowest energy conformations which are *tg* and *gt* in the case of an isotactic dyad and *tt* in the case of a syndiotactic dyad. This process is illustrated for an isotactic dyad in Figure 8, parts b−d. The first excimer is therefore formed less rapidly than the second, and the magnitude of the activation energy for its formation is expected to be similar to that for the segmental motion of the PNVC chain. However, as Abe et al.[34] have pointed out, the conformational properties of electronically excited PNVC may be rather different from those of the unexcited molecule because of different interaction energies between excited and unexcited carbazole groups.

Although tacticity appears to play a major role in the formation of the two types of excimers, the NMR relaxation data presented here are relatively insensitive to the chain stereochemistry, as noted above. It appears

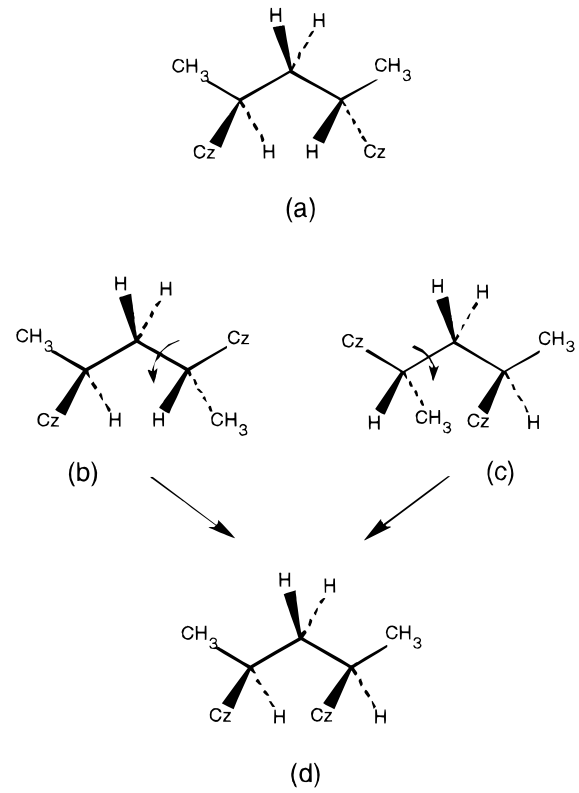

Figure 8. (a) Ground state conformation (*tt*) of *racemic* 2,4-di-*N*-carbazolyl pentane. (b and c) Ground state conformations (*tg*) and (*gt*) of *meso*-2,4-di-*N*-carbazolylpentane; (d) Excited state conformation (*tt*) of *meso*-2,4-di-*N*-carbazolylpentane, which forms the true excimer.

that the shape of the conformational potential energies at the minima and maxima of the various conformations are similar for different stereochemical sequences. It should be noted that the T_1 and NOE data sample numerous conformations and dynamic processes of the PNVC backbone and thus it is not peculiar that the values are insensitive to tacticity. Nevertheless, the motional behavior of PNVC described using the DLM model should give some indication of the effect of chain local dynamics on the excimer formation. Since internal rotation of the carbazole group is highly restricted, segmental dynamics will be considered. According to the DLM model, the backbone motions are described in terms of isolated, single conformational transitions with correlation time τ_0, and cooperative conformational transitions with correlation time τ_1. The correlation time τ_0 may compared with the rate of formation of the true excimer, since the sandwich-like disposition of the two carbazole rings requires rotation about a single C−C bond. τ_1 is expected to influence the formation of the second excimer, since cooperative conformational transitions are characterized by a torsional angle less than 120°.

These correlation times should be compared with the rates of excimer formation. If these correlation times are comparable or smaller than the rate of the excimer formation, then the electronic excitation arrives at site in which two carbazole groups have achieved the proper geometry that favors the excimer formation. On the other hand, larger correlation times than the rate of the excimer formation reflect the insensitivity of the chain local dynamics on the polymer photophysical behavior. Ng and Guillet[4] have analyzed the fluorescence decay

of PNVC in dilute benzene solutions at 24 °C, estimating the lifetimes (defined as total depopulation rate of excimer) of the true and the second excimers as 12.8 and 2.9 ns, respectively. In THF at room temperature,[2] these values were found to be 17 and 4 ns, and another study[36] in the same solvent and temperature found values of 11.5 and 2.5 ns. The correlation times τ_0 and τ_1 in THF at room temperature are ∼1 and ∼30 ns respectively (Table 1), comparable to the lifetimes of the two types of excimers formed in the PNVC chain. Although, no experimental data exist in other solvents for the excimer lifetimes of PNVC, it appears to be the segmental motion of the polymer backbone, but not the side-chain motion, which influences the excimer formation.

IV. Conclusions

Carbon-13 relaxation measurements have been performed for the protonated carbons of poly(*N*-vinylcarbazole) in five solvents. Correlation times describing segmental chain motions in dilute solutions have been extracted from the relaxation data by using the DLM bimodal time-correlation function. The correlation times were found to be proportional to the solvent viscosity, η, whether the viscosity is varied by changing the temperature or the solvent. This result is in agreement with predictions of the Kramers' theory describing the hydrodynamic behavior of PNVC in the high-friction limit. The internal energy barrier E^* associated with C−H vector orientation was found to be 9.1 ± 0.3 kJ mol^{-1}. The success of the DLM model and Kramers' theory in describing the conformational dynamics and the hydrodynamic behavior of the PNVC polymer, respectively, has been confirmed by applying the frequency−temperature superposition principle to the T_1 and NOE data of the backbone carbons. Finally, the relaxation data of the protonated aromatic carbons of the carbazole group showed that the carbazole internal motion about the C−N bond is highly restricted.

Acknowledgment. We gratefully acknowledge financial support from the General Secretariat for Research and Technology of Greece, the British Council and NATO (Grant No. CRG 9600593).

References and Notes

(1) Johnson, G. E. *J. Chem. Phys.* **1975**, *62*, 4697.
(2) Itaya, A.; Okamoto, K.; Kusabayashi, S. *Bull. Chem. Soc. Jpn.* **1976**, *49*, 2082.
(3) Block, H. *Adv. Polym. Sci.* **1979**, *33*, 93.
(4) Ng, D.; Guillet, J. E. *Macromolecules* **1981**, *14*, 405.
(5) Solaro, R.; Galli, G.; Ledwith, A.; Chiellini, E. In *Polymer Photophysics*; Phillips, D., Ed.; Chapman and Hall: London, 1985; Chapter 8.
(6) Sakai, H.; Itaya, A.; Masuhara, H.; Sasaki, K.; Kawata, S. *Polymer* **1996**, *37*, 31.
(7) Davidson, K. Soutar, I.; Swanson, L.; Yin, J. *J. Polym. Sci., Part B: Polym. Phys.* **1997**, *35*, 963.
(8) Spyros, A.; Dais, P. *Macromolecules* **1992**, *25*, 1062.
(9) Spyros, A.; Dais, P.; Heatley, F. *Macromolecules* **1994**, *27*, 5845.
(10) Radiotis, T.; Spyros, A.; Dais, P. *Polymer* **1993**, *34*, 1846.
(11) Spyros, A.; Dais, P.; Heatley, F. *Macromolecules* **1994**, *27*, 6207.
(12) Viswanath, D. S.; Natarajan, G. *Databook on the Viscosity of Liquids*; Hemisphere Publishing: New York, 1988.
(13) *Zahlenwerte und Funktionen*; Springer-Verlag: Berlin, 1969; Band II, Teil 5, Vol. 5, p 215.
(14) Craik, D. J.; Kumar, A.; Levy, G. C. *J. Chem. Inf. Comput. Sci.* **1983**, *23*, 30.
(15) Dais, P. *Carbohydr. Res.* **1987**, *160*, 73.
(16) Gaussian 94 (Revision D.4), Frisch, M. J.; Trucks, G. W.; Schlegel, H. B.; Gill, P. M. W.; Johnson, B. G.; Robb, M. A.; Cheeseman, J. R.; Keith, T.; Petersson, G. A.; Montgomery, J. A.; Raghavachari, K.; Al-Laham, M. A.; Zakrzewski, V. G.; Ortiz, J. V.; Foresman, J. B.; Cioslowski, J.; Stefanov, B. B.; Nanayakkara, A.; Challacombe, M.; Peng, C. Y.; Ayala, P. Y.; Chen, W.; Wong, M. W.; Andres, J. L.; Replogle, E. S.; Gomperts, R.; Martin, R. L.; Fox, D. J.; Binkley, J. S.; Defrees, D. J.; Baker, J.; Stewart, J. P.; Head-Gordon, M.; Gonzalez, C.; Pople, J. A. Gaussian, Inc., Pittsburgh, PA, 1995.
(17) Dais, P.; Spyros, A. *Prog. Nucl. Magn. Reson. Spectrosc.* **1995**, *27*, 555.
(18) Heatley, F. *Prog. Nucl. Magn. Reson. Spectrosc.* **1979**, *13*, 47.
(19) Gisser, D. J.; Glowinkowski, S.; Ediger, M. D. *Macromolecules* **1991**, *24*, 4270.
(20) Kupka, T.; Pasterna, G.; Jaworska, M.; Karali, A.; Dais, P. *Magn. Reson. Chem* **2000**, *38*, 149.
(21) Dejean de la Batie, R.; Lauprêtre, F.; Monnerie, L. *Macromolecules* **1988**, *21*, 2045.
(22) Tylianakis, E. I.; Dais, P.; Heatley, F. *J. Polym. Sci.: Part B: Polym. Phys.* **1997**, *35*, 317.
(23) Moe, N. E.; Qiu, X.; Ediger, M. D. *Macromolecules* **2000**, *33*, 2145.
(24) Moe, N. E.; Ediger, M. D. *Macromolecules* **1995**, *28*, 2329.
(25) Monnerie, L. *J. Non-Cryst. Solids* **1991**, *131*−*133*, 755.
(26) Zhu, W.; Ediger, M. D. *J. Polym. Sci., Part B: Polym. Phys. Ed.* **1997**, *35*, 1241.
(27) Glowinkowski, S.; Gisser, D. J.; Ediger, M. D. *Macromolecules* **1990**, *23*, 3520.
(28) Kramers, A. H. *Physica* **1940**, *7*, 284.
(29) Zhu, W.; Ediger, M. D. *Macromolecules* **1997**, *30*, 1205.
(30) Zhu, W.; Gisser, D. J.; Ediger, M. D. *J. Polym. Sci., Part B: Polym. Phys.* **1994**, *32*, 2251.
(31) Guillermo, A.; Dupeyre, R.; Cohen-Addad, J. P. *Macromolecules* **1990**, *23*, 1291.
(32) Karali, A.; Froudakis, G. E.; Dais, P.; Heatley, F. *Macromolecules*, in press.
(33) Johnson, G. E..; Good, A. T. *Macromolecules* **1982**, *15*, 409.
(34) Abe, A.; Kobayashi, H.; Kawamura, T.; Date, M.; Uryu, T.; Matsuzaki, K. *Macromolecules* **1988**, *21*, 3414.
(35) Sundararajan, P. R. *Macromolecules* **1980**, *13*, 512.
(36) Roberts, A. J.; Cureton, C. G.; Phillips, D. *Chem. Phys. Lett.* **1980**, *72*, 554.

MA000092C